Development of Consistent Kinetic Models Derived from a Microkinetic Model of the Methanol Synthesis

Bruno Lacerda de Oliveira Campos, Karla Herrera Delgado,* Stephan Pitter, and Jörg Sauer

ABSTRACT: In this work, a recently published microkinetic model of the methanol synthesis and the water gas shift reaction on Cu/Zn based catalysts is used to develop three particularly interesting formal kinetic models, drastically reducing model complexity. In the first model, kinetic parameters are taken from DFT data used in the microkinetic mechanism, and only a single parameter is fitted to experiments. Still, this model adequately simulates experiments with low to moderate CO_2 content in feed mixtures. A second model, which has an increased amount of estimated parameters (nine in total), performs well for the whole range of studied operating conditions. At last, a third model, which has six fitted parameters and neglects CO hydrogenation, adequately simulates conditions with CO_2 containing feed. Each developed kinetic model is either equally well or better suited for the simulation of methanol synthesis than literature models with a higher amount of parameters.

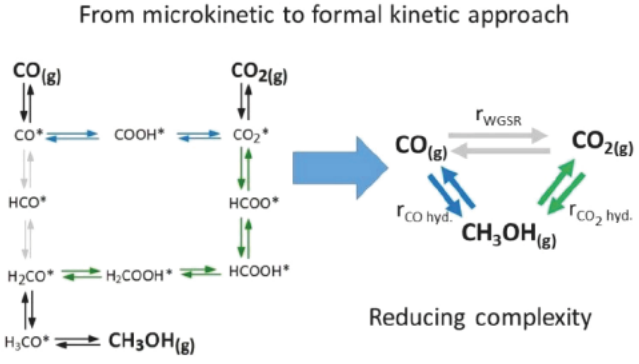

1. INTRODUCTION

Catalytic methanol synthesis is an important process in the chemical industry. Its relevance has increased in recent years, since it is an intermediate step in the production of liquid fuels and chemicals from sustainably derived hydrogen and CO/CO_2, while also being a relevant energy carrier itself.[1,2]

Typically, industrial methanol synthesis is performed at 50−100 bar and 200−300 °C on $Cu/ZnO/Al_2O_3$ catalysts.[3] Three main reactions occur: CO hydrogenation to methanol, CO_2 hydrogenation to methanol and the water gas shift reaction (WGSR).

$$CO_{(g)} + 2H_{2(g)} \rightleftarrows CH_3OH_{(g)} \quad \Delta H^0_{25°C} = -90.6\ \text{kJ mol}^{-1} \tag{1}$$

$$CO_{2(g)} + 3H_{2(g)} \rightleftarrows CH_3OH_{(g)} + H_2O_{(g)} \quad \Delta H^0_{25°C} = -49.4\ \text{kJ mol}^{-1} \tag{2}$$

$$CO_{(g)} + H_2O_{(g)} \rightleftarrows CO_{2(g)} + H_{2(g)} \quad \Delta H^0_{25°C} = -41.0\ \text{kJ mol}^{-1} \tag{3}$$

Different formal kinetic models have been proposed to describe the methanol synthesis based on these reactions. Graaf et al.[4] proposed a model assuming direct hydrogenation of both CO and CO_2 as relevant, and two different active sites. Vanden Bussche and Froment[5] followed the same approach for the active sites, but neglected CO direct hydrogenation, which reduced the total parameter number to nine. Seidel et al.[6] considered both types of hydrogenation, three different active sites, and dynamic structural changes of the catalyst surface which Ovesen et al.[7] proposed. Slotboom et al.[8] also assumed three different active sites, but neither considered CO direct hydrogenation nor structural changes, deriving a model with six parameters.

An alternative approach is microkinetic modeling,[9−14] which is based on theoretical calculations, such as density functional theory,[15−17] and considers all intermediate reaction steps as potentially limiting. In general, it is believed that microkinetic models are more suitable to extrapolations than formal kinetic models, since in the latter approach different effects might be merged with kinetic parameters.[18] However, the implementation of microkinetic models is complex, and the simulations require higher computational effort comparing to formal kinetic models.

To get the advantages of both formal and microkinetic approaches, it is, therefore, of interest to extract the relevant theoretical information on a microkinetic model and implement a simpler and faster computing model.[19] One strategy is to make use of sensitivity analyses, for example, the degree of rate control

Table 1. Operating Conditions of the Different Setups Considered

database	pressure (bar)	temp (°C)	GHSV (L h^{-1} $g_{cat.}^{-1}$)	Feed concn (% v/v) H_2	CO	CO_2	N_2
Campos[14]	40 60	210 260	24 40	20 60	3 30	1.3 20	20 50
Seidel[6]	30 70	230 260	3.6	60 76	0 21	0 13	15 16
Slotboom[8]	20 50	178 260	1.3 6.5	66 80	0	12 25	0 11

Table 2. Estimated Parameters and Considered Experimental Data for Each Model

model	no. of parameters	parameter description	no. of points training	validation	considered database
Model-1p	1	$n_{M,Cat}$	445	112	all points
Model-6p	6	A_{2-3}, $E_{A,2-3}$, $\overline{K}_{2-3}$	397	99	only points with $\overline{y}_{CO_2,0} \geq 0.001$
Model-9p	9	A_{1-3}, $E_{A,1-3}$, $\overline{K}_{1-3}$	445	112	all points
Seidel	12	$k_{CO}(A,B)$, $k_{CO_2}(A,B)$, $k_{rWGSR}(A,B)$, K_{CO}, $\frac{K_{H_2O}K_O}{K_{H_2}}$, k_{CO_2}, K_{H_2O}, $\sqrt{K_{H_2}}$, ΔG_3	445	112	all points
Slotboom A	6	$k_{CO_2}(a,b)$, $k_{rWGSR}(a,b)$ K_{H_2}, $K_{H_2O/9}$	445	112	all points
Slotboom B	6	$k_{CO_2}(a,b)$, $k_{rWGSR}(a,b)$ K_{H_2}, $K_{H_2O/9}$	397	99	only points with $\overline{y}_{CO_2,0} \geq 0.001$

(DRC),[20] to assume rate determining steps (RDS), and to derive reaction rate equations. Since the parameters from these kinetic equations are known, the developed model will need less fitted parameters (or even none) comparing with common formal kinetic models.

In this work, a fast computing formal kinetic model (Model 1p) is derived from our previously proposed microkinetic model of the methanol synthesis.[14] Two additional models are also proposed (Model 9p and Model 6p), the parameters of which are lumped and re estimated. All three proposed models are compared with state of the art literature models.[6,8]

2. DEVELOPMENT OF THE KINETIC MODELS

In this section, the derivation of the models and the parameter estimation are described.

2.1. Model-1p: Direct Reduction of the Microkinetic Model. In our recent work,[14] a microkinetic model for the methanol synthesis and the WGSR was proposed based on first principles Density Functional Theory (DFT) calculations.[16,17] The model consists of a total of 25 reversible reactions and 23 surface species, and has a three site approach: two for carbon containing compounds (site a, pure Cu; site b, Cu/Zn) and one exclusively for hydrogen and water adsorption (site c). Five main reaction pathways were considered, which are described in Table S1.

In Model 1p, global reactions are derived from the elementary reactions listed in Table S1 by assuming rate determining steps (RDS) for each reaction path. From the DRC analysis, our findings showed that $HCO_{(a)}$ formation (R_{11}) is the most sensitive step of CO hydrogenation.[14] By considering R_{11} as the RDS, and assuming the other elementary steps to be in equilibrium, the reaction rate for CO hydrogenation is derived:

$$r_{CO} = n_{M,Cat} k_{11}^{+} (1 - \phi_{Zn}) \theta_a \theta_c K_1 K_2 K_{10} f_{H_2} f_{CO} \times \left(1 - \frac{f_{CH_3OH}}{f_{H_2}^2 f_{CO} K_{P,COhyd}^0}\right) \quad (4)$$

where $n_{M,Cat}$ is the quantity of active sites (mol·kg_{cat}^{-1}), k_{11}^{+} is the kinetic constant of the forward reaction 11, ϕ_{Zn} is the zinc coverage on the catalyst surface, θ_a and θ_c are the surface coverage of free sites (a) and (c), respectively, K_k is the equilibrium constant of elementary reaction k, f_j is the fugacity of gas component j, and $K_{P,CO\ hyd}^0$ is the equilibrium constant of the global CO hydrogenation. The fugacities of the gases are given in bars, so that the division by the reference pressure (1 bar) can be omitted.

CO_2 hydrogenation is only active on site (b),[17] and formic acid ($HCOOH_{(b)}$) hydrogenation (R_{17}) is the most sensitive step of CO_2 hydrogenation, according to our DRC analysis.[14] Therefore, the reaction rate of the CO_2 hydrogenation is

Table 3. Comparison of Statistical Values for the Different Kinetic Models That Consider the Whole Studied Operating Region ($0 \leq y_{CO_2,0} \leq 1$)

	Model-1p	Model-9p	Microkin.[a]	Slotboom A	Seidel
no. of fitted parameters	1	9	1	6	12
χ^2 all points (557 pts)	69.3	22.3		62.6	24.7
χ^2 feed: H_2/CO (61 pts)	9.6	3.4	9.3	5.1	4.1
χ^2 feed: H_2/CO/CO_2 (370 pts)	14.1	7.4	13.6	47.2	9.0
χ^2 feed: H_2/CO_2 (126 pts)	45.5	11.5	35.3	10.3	11.6
$\chi^2_{Orig.\ Par.}$ all points (557 pts)			58.2	270.9	144.2
MSE all points	0.0430	0.0138	0.0361	0.0387	0.0153
MSE feed: H_2/CO (61 pts)	0.0781	0.0280	0.0764	0.0414	0.0339
MSE feed: H_2/CO/CO_2 (370 pts)	0.0127	0.0066	0.0123	0.0425	0.0081
MSE feed: H_2/CO_2 (126 pts)	0.1200	0.0304	0.0934	0.0274	0.0306
MSE training (80% of the pts)	0.0398	0.0131		0.0395	0.0142
MSE validation (20% of the pts)	0.0557	0.0167		0.0363	0.0198

[a]No parameter re estimation is made for the microkinetic model.

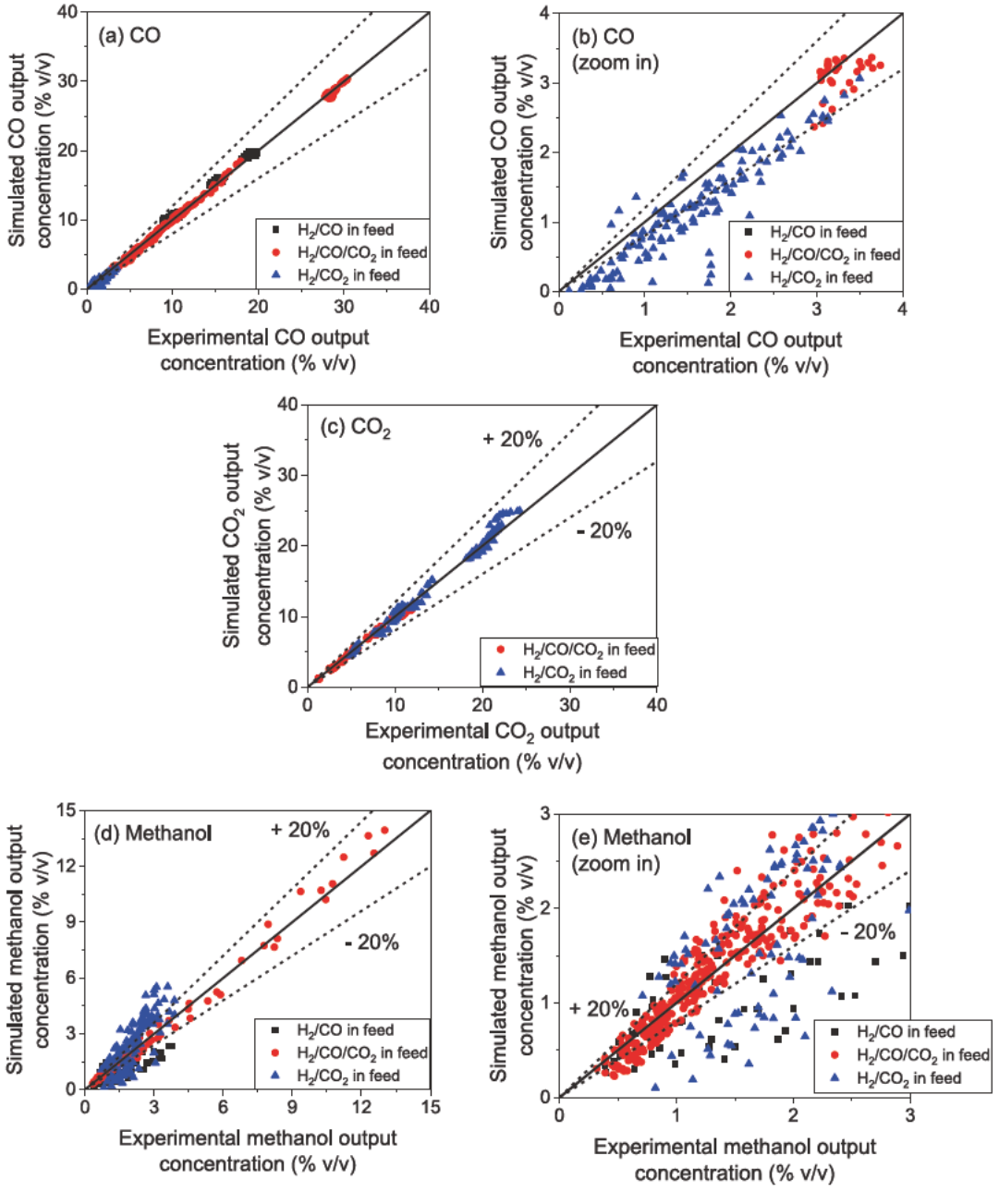

Figure 1. Parity plots of Model 1p for measured and predicted CO (a, b), CO_2 (c), and methanol (d, e) concentrations in the product stream. Experimental conditions are reported in Table 1.

$$r_{CO_2} = n_{M,Cat} k_{17}^{+} \phi_{Zn} \theta_b \theta_c K_1^{1.5} K_5 K_{13} K_{15} f_{H_2}^{1.5} f_{CO} \times \left(1 - \frac{f_{CH_3OH} f_{H_2O}}{f_{H_2}^3 f_{CO_2} K_{P,CO_2hyd}^0}\right) \quad (5)$$

$$r_{rWGSR} = n_{M,Cat} k_{24}^{-} \theta_c K_8 [(1 - \phi_{Zn}) \theta_a K_4 + \phi_{Zn} \theta_b K_5] f_{CO_2} f_{H_2O} \times \left(1 - \frac{f_{CO} f_{H_2O}}{f_{H_2} f_{CO_2} K_{P,rWGSR}^0}\right) \quad (6)$$

where θ_b is the surface coverage of free sites (b).

According to our DRC analysis, the carboxyl formation (COOH*) (R_{24} and R_{25}) are the most sensitive steps for the reverse WGSR (rWGSR) on sites (a) and (b), respectively, and $k_{24}^{-} = k_{25}^{-}$.[14] The reaction rate of the rWGSR (sum of the reactions happening on both sites) is

One might find strange that water is positively influencing the rWGSR. But this is because the water assisted carboxyl mechanism is considered (see Table S1). Detailed mathematical derivation of the global kinetic equations from the elementary reactions is available in the Supporting Information.

The fugacity coefficients are calculated through the Peng Robinson equation,[21] using binary interaction parameters and other necessary information from literature,[22,23] including an effective hydrogen acentric factor of −0.05.[24] The reaction rate and equilibrium constants are calculated as follows:

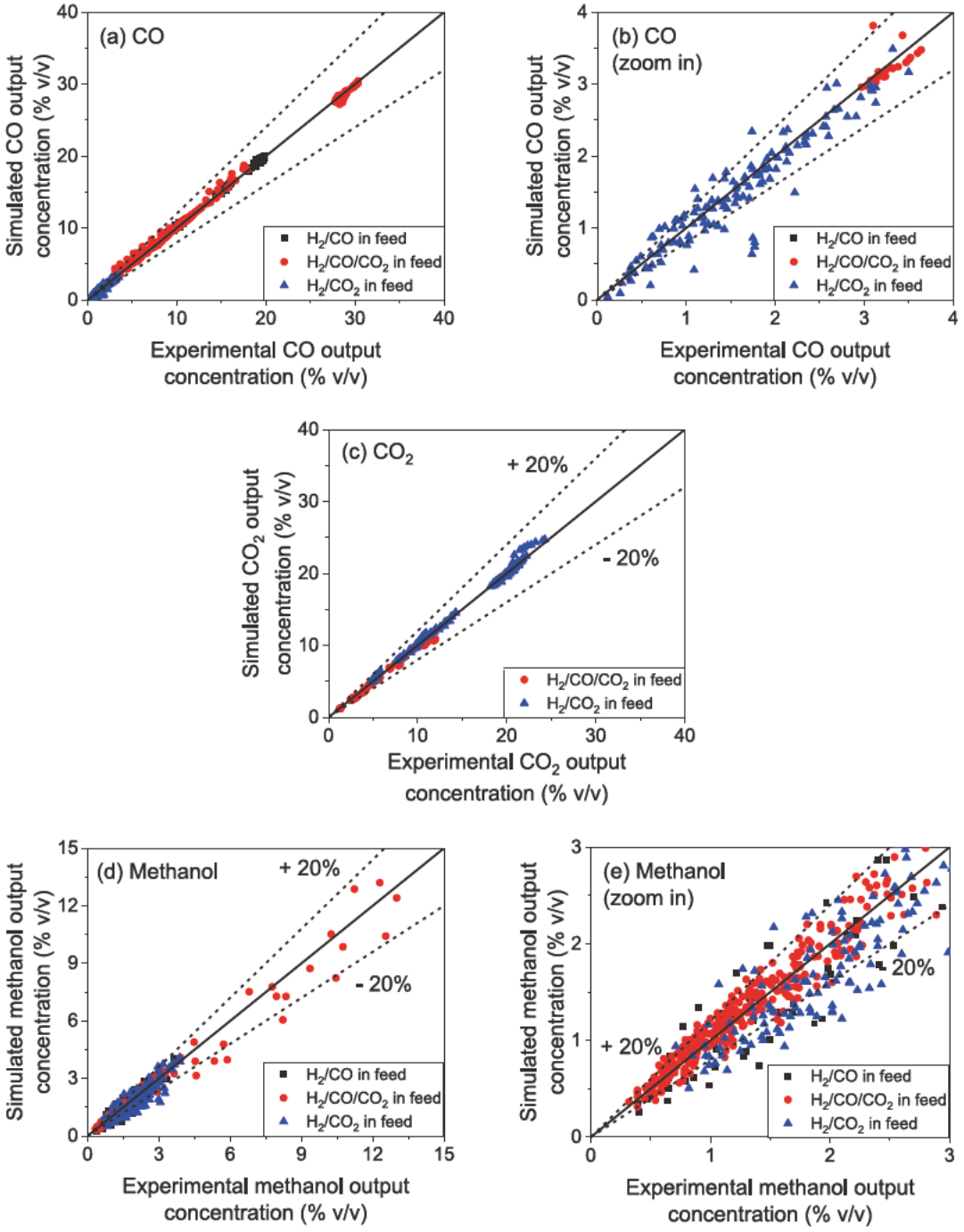

Figure 2. Parity plots of Model 9p for measured and predicted CO (a, b), CO_2 (c), and methanol (d, e) concentrations in the product stream. Experimental conditions are reported in Table 1.

$$k_k^+ = \frac{k_b}{\hbar} T^{(1+\beta_k^+)} \exp\left[\frac{\Delta S_k^{\ddagger,+}}{R} - \frac{E_{A,k}^+}{RT}\right] \tag{7}$$

$$K_k = \frac{k_k^+}{k_k^-} = T^{(\beta_k^+ - \beta_k^-)} \exp\left[\frac{(\Delta S_k^{\ddagger,+} - \Delta S_k^{\ddagger,-})}{R} - \frac{(E_{A,k}^+ - E_{A,k}^-)}{RT}\right] \tag{8}$$

$$K_{P,m}^0 = \exp\left(\frac{-\Delta G_{\text{reaction}\,m}^0}{RT}\right) = \exp\left[-\frac{1}{R}\left(\frac{A_{1,m}}{T} + A_{2,m} + A_{3,m}\Delta \ln T\right)\right] \tag{9}$$

Here, k_b is the Boltzmann constant, $\hbar$ is the Planck constant, β is a constant used due to the thermodynamic consistency process,[14,25,26] $\Delta S^{\ddagger}$ is the entropy barrier, E_A is the activation energy, $\Delta G_{reaction\ m}^0$ is the free Gibbs energy variation of the global reaction, and $A_{1-3,m}$ is the estimated parameters for the

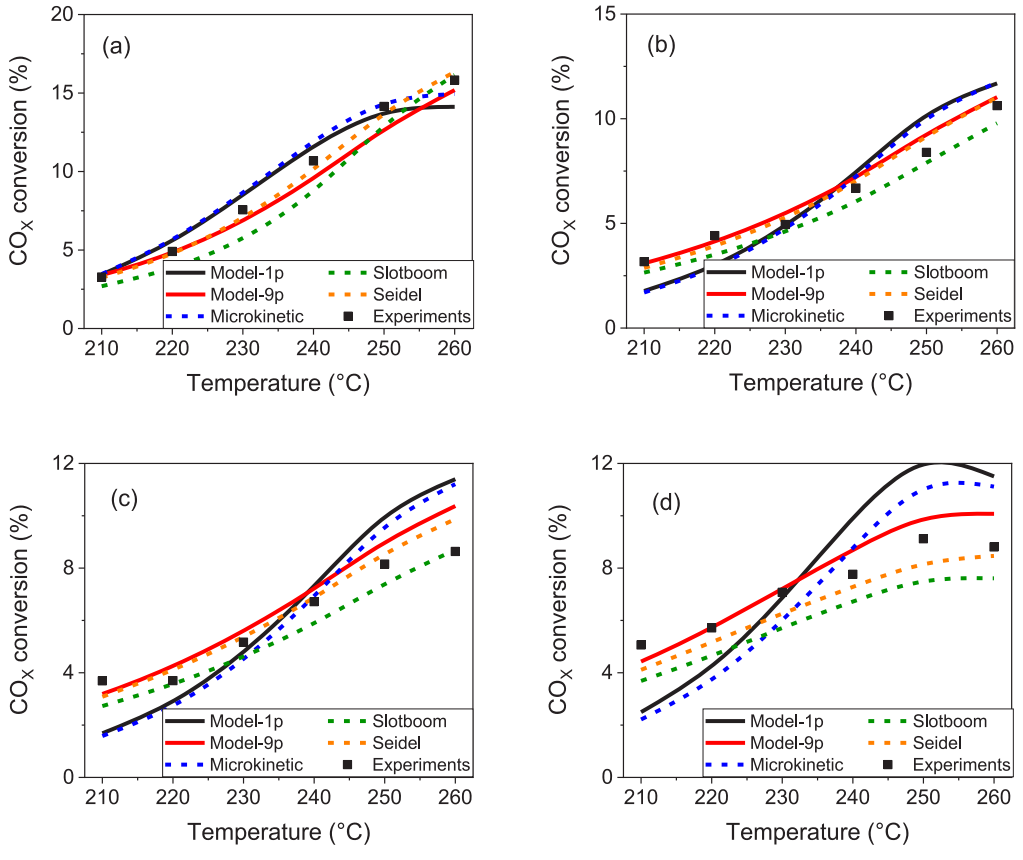

Figure 3. CO_X conversion: simulation vs experiments reported by Campos et al.[14] Conditions: All experiments were performed at 41 bar. (a) GHSV = 24 $L{\cdot}h^{-1}{\cdot}g_{cat}^{-1}$, $H_2/CO/CO_2$ (feed) = 45.3/11.7/2.7% v/v. (b) GHSV = 40 $L{\cdot}h^{-1}{\cdot}g_{cat}^{-1}$, $H_2/CO/CO_2$ (feed) = 45.3/8.9/5.6% v/v. (c) GHSV = 40 $L{\cdot}h^{-1}{\cdot}g_{cat}^{-1}$, $H_2/CO/CO_2$ (feed) = 45.2/8.9/8.8% v/v. (d) GHSV = 24 $L{\cdot}h^{-1}{\cdot}g_{cat}^{-1}$, $H_2/CO/CO_2$ (feed) = 45.2/4.3/10.4% v/v.

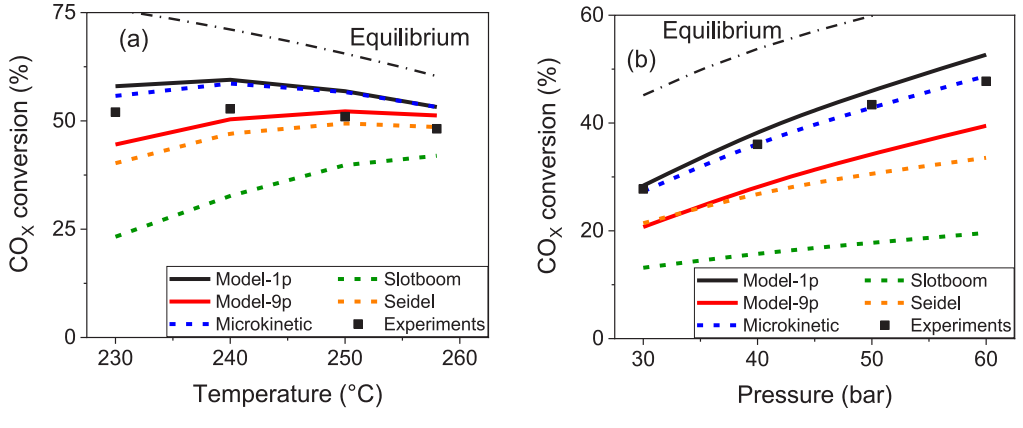

Figure 4. CO_X conversion: simulation vs experiments reported by Seidel et.al.[6] All experiments are at GHSV = 3.6 $L{\cdot}h^{-1}{\cdot}g_{cat}^{-1}$. (a) 60 bar, $H_2/CO/CO_2$ (feed) = 69.5/11.6/3.2% v/v. (b) 230 °C, $H_2/CO/CO_2$ (feed) = 69.6/8.2/5.7% v/v.

equilibrium constant.[14,27] The superscripts "+" and "−" refer to forward and reverse reaction k, respectively.

The free sites (a), (b), and (c) are calculated from the sites balance eqs (eqs 10−12). The simulations with the microkinetic model showed that only $CO_{(a)}$, $HCOO_{(a)}$, $HCOO_{(b)}$, $H_3CO_{(b)}$, $H_{(c)}$, $OH_{(c)}$, (a), (b), and (c) have significant coverage values.[14] That is, 0.05 or more in at least one of the various conditions tested. Therefore, the other species are neglected in the sites balance.

$$\theta_a = (K_2 f_{CO} + K_1^{0.5} K_4 K_{12} f_{H_2}^{0.5} f_{CO_2} + 1)^{-1} \quad (10)$$

$$\theta_b = (K_1^{0.5} K_5 K_{13} f_{H_2}^{0.5} f_{CO_2} + K_1^{-0.5} K_7^{-1} f_{H_2}^{-0.5} f_{CH_3OH} + 1)^{-1} \quad (11)$$

$$\theta_c = (K_1^{0.5} f_{H_2}^{0.5} + K_1^{-0.5} K_8 K_9 f_{H_2}^{-0.5} f_{H_2O} + 1)^{-1} \quad (12)$$

It is also known that the surface of Cu/Zn based catalysts changes depending on the operating conditions (i.e., gas composition and temperature), and the zinc coverage generally decreases with an increase in the CO_2 to CO_x ratio (CO_x = CO + CO_2).[28]

Ovesen et al.[7] proposed a method to estimate the zinc coverage based on Wulff constructions, in which a parameter has

to be fitted to the experiments. Kuld et al.[29] proposed a detailed method to describe the zinc coverage based on DFT calculations, which takes different effects into account (e.g., lower atom coordination in ZnO nanoparticles, Zn−Zn interaction energy reducing the segregation energies, etc.). With this second method, the computational effort to solve the model is significantly increased, due to the need to numerically solve a highly nonlinear equation at each integration step. In the microkinetic model,[14] the estimation of the zinc coverage (ϕ_{Zn}) was initially based on the method developed by Kuld et al.[29] but later the estimation based on a third method was recommended instead, because it led to a more accurate simulation of the experiments.[14,30]

The third method consists of giving constant zinc coverage values depending on the CO_2 to CO_x ratio in feed mixture, named here $y_{CO_2,0}$. The reference case is equal amounts of active copper and zinc on the surface (ϕ_{Zn} = 0.50). For the case without CO_2 in feed ($y_{CO_2,0} \leq 0.001$), an upper limit of ϕ_{Zn} = 0.95 is settled.[14] Finally, for the case of very high CO_2 in feed ($y_{CO_2,0} > 0.90$), a lower limit of ϕ_{Zn} = 0.10 is given. The different methods were tested with the new formal kinetic models, and the experiments were more accurately simulated with the third method. Since this method has the lowest computational effort and does not require extra fitting parameters, it was chosen for the kinetic models presented here.

The Model 1p is a reduced version of the microkinetic mechanism, being also based on data from DFT calculations. Therefore, only one parameter, the quantity of active sites ($n_{M,Cat}$), is to be estimated with experimental data. All other parameters, summarized in Table S3, are directly transferred from the microkinetic model.[14]

2.2. Model-9p: Fitting the Lumped Parameters. In Model 9p, the same reaction network of Model 1p is considered, but the parameters are lumped and fitted to experiments instead of taken from DFT calculations. The objective of setting up this model is to correlate the simulations and experimental data with the smallest deviation possible. To reduce the amount of parameters to be estimated, beta terms of eqs 7 and 8 are neglected ($\beta_k^+, \beta_k^- = 0$), as these are not necessary to ensure the thermodynamic consistency of the model. The derived reaction rate equations (eqs 13−15) are as follows:

$$r_{CO} = \exp\left(A_1 - \frac{E_{A,1}}{RT}\right)(1 - \phi_{Zn})\theta_a\theta f_{H_2} f_{CO} \times \left(1 - \frac{f_{CH_3OH}}{f_{H_2}^2 f_{CO} K_{P,CO\,hyd}^0}\right) \quad (13)$$

$$r_{CO_2} = \exp\left(A_2 - \frac{E_{A,2}}{RT}\right)\phi_{Zn}\theta_b\theta f_{H_2}^{1.5} f_{CO} \times \left(1 - \frac{f_{CH_3OH} f_{H_2O}}{f_{H_2}^3 f_{CO_2} K_{P,CO_2hyd}^0}\right) \quad (14)$$

$$r_{rWGSR} = \exp\left(A_3 - \frac{E_{A,3}}{RT}\right)\theta_c[(1 - \phi_{Zn})\theta_a + \phi_{Zn}\theta_b] f_{CO_2} f_{H_2O} \times \left(1 - \frac{f_{CO} f_{H_2O}}{f_{H_2} f_{CO_2} K_{P,rWGSR}^0}\right) \quad (15)$$

Here, A_{1-3} are pre exponential factors and $E_{A,1-3}$ are global activation energies, which are parameters to be fitted to the experiments and correspond to the lumping of the following terms (contained in Model 1p):

$$A_1 = \ln\left(n_{M,Cat}\frac{k_b}{\hbar}\right) + \frac{\Delta S_{11}^{\ddagger,+} + \Delta S_1^{\ddagger,+} - \Delta S_1^{\ddagger,-} + \Delta S_2^{\ddagger,+} - \Delta S_2^{\ddagger,-} + \Delta S_{10}^{\ddagger,+} - \Delta S_{10}^{\ddagger,-}}{R} \quad (16)$$

$$A_2 = \ln\left(n_{M,Cat}\frac{k_b}{\hbar}\right) + \frac{\Delta S_{17}^{\ddagger,+} + 1.5(\Delta S_1^{\ddagger,+} - \Delta S_1^{\ddagger,-}) + \Delta S_5^{\ddagger,+} - \Delta S_5^{\ddagger,-}}{R} + \frac{\Delta S_{13}^{\ddagger,+} - \Delta S_{13}^{\ddagger,-} + \Delta S_{15}^{\ddagger,+} - \Delta S_{15}^{\ddagger,-}}{R} \quad (17)$$

$$A_3 = \ln\left(n_{M,Cat}\frac{k_b}{\hbar}\right) + \frac{\Delta S_{24}^{\ddagger,-} + \Delta S_8^{\ddagger,+} - \Delta S_8^{\ddagger,-} + \Delta S_4^{\ddagger,+} - \Delta S_4^{\ddagger,-}}{R} \quad (18)$$

$$E_{A,1} = \frac{E_{A,11}^+ + E_{A,1}^+ - E_{A,1}^- + E_{A,2}^+ - E_{A,2}^- + E_{A,10}^+ - E_{A,10}^-}{R} \quad (19)$$

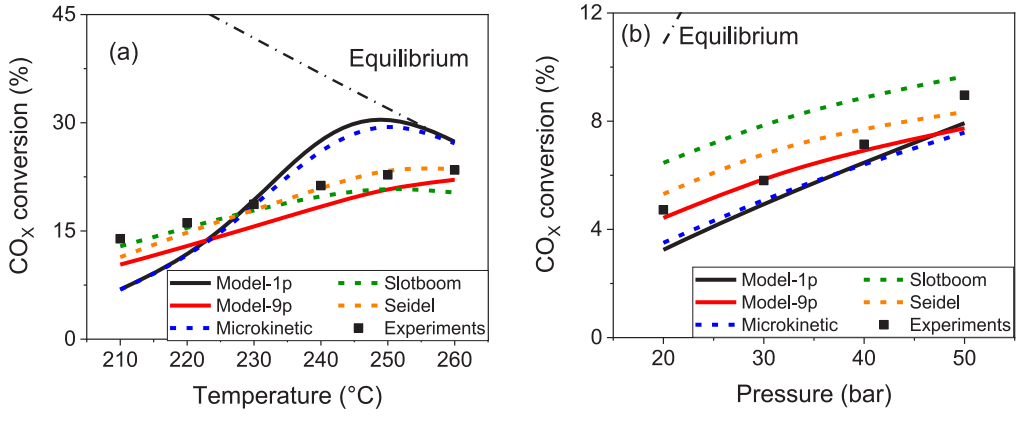

Figure 5. CO_X conversion: simulation vs experiments reported by Slotboom et al.[8] All experiments are at H_2/CO_2 (feed) = 67.5/22.3%. (a) 50 bar, GHSV = 3.9 L·h^{-1}·g$_{cat}^{-1}$. (b) 220 °C, GHSV = 2.6 L·h^{-1}·g$_{cat}^{-1}$.

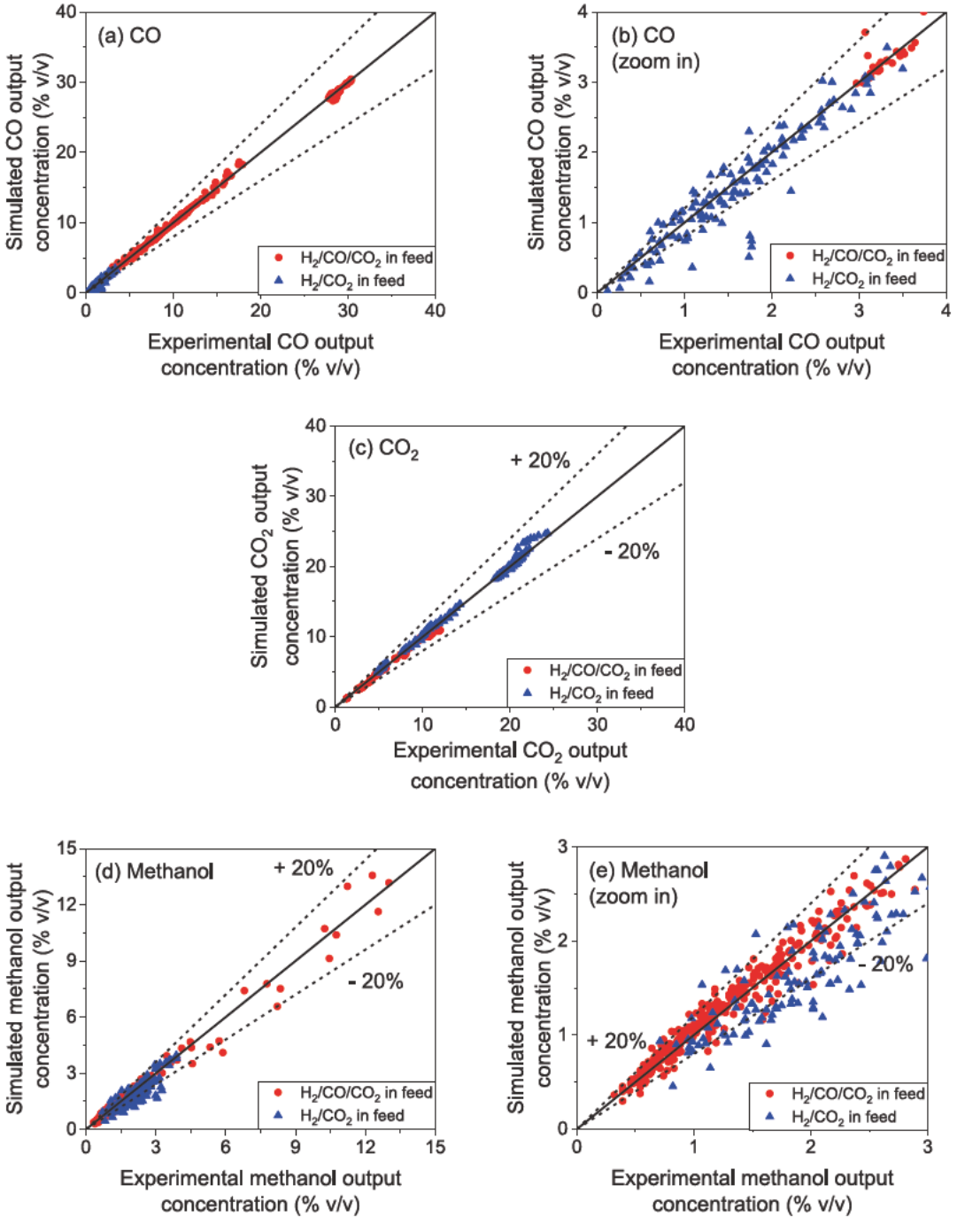

Figure 6. Parity plots of Model 6p for measured and predicted CO (a,b), CO_2 (c), and methanol (d,e) concentrations in the product stream. Experimental conditions are all points reported in Table 1 that contain CO_2 in feed.

$$E_{A,2} = \frac{E_{A,17}^{+,+} + 1.5(E_{A,1}^{+} - E_{A,1}^{-}) + E_{A,5}^{+} - E_{A,5}^{-} + E_{A,13}^{+} - E_{A,13}^{-} + E_{A,15}^{+} - E_{A,15}^{-}}{R} \quad (20)$$

$$E_{A,3} = \frac{E_{A,24}^{-} + E_{A,8}^{+} - E_{A,8}^{-} + E_{A,4}^{+} - E_{A,4}^{-}}{R} \quad (21)$$

From the microkinetic model simulations,[14] it was seen that $CO_{(a)}$, $H_3CO_{(b)}$, and $H_{(c)}$ rarely achieve coverages greater than 0.07, and therefore, have limited influence in the sites balance when compared to $HCOO_{(a)}$, $HCOO_{(b)}$, $OH_{(c)}$. Therefore, to further reduce the amount of parameters to be estimated, only $HCOO_{(a)}$, $HCOO_{(b)}$, $OH_{(c)}$, (a), (b), and (c) are considered in the sites balance, described as follows.

$$\theta_a = (\overline{K_1} f_{H_2}^{0.5} f_{CO_2} + 1)^{-1} \quad (22)$$

$$\theta_b = (\overline{K_2} f_{H_2}^{0.5} f_{CO_2} + 1)^{-1} \quad (23)$$

$$\theta_c = (\overline{K_3} f_{H_2}^{-0.5} f_{H_2O} + 1)^{-1} \quad (24)$$

where K_{1-3} are the lumped parameters related to the formation of $HCOO_{(a)}$, $HCOO_{(b)}$, and $OH_{(c)}$, which need to be estimated. These parameters, often called adsorption constants, represent

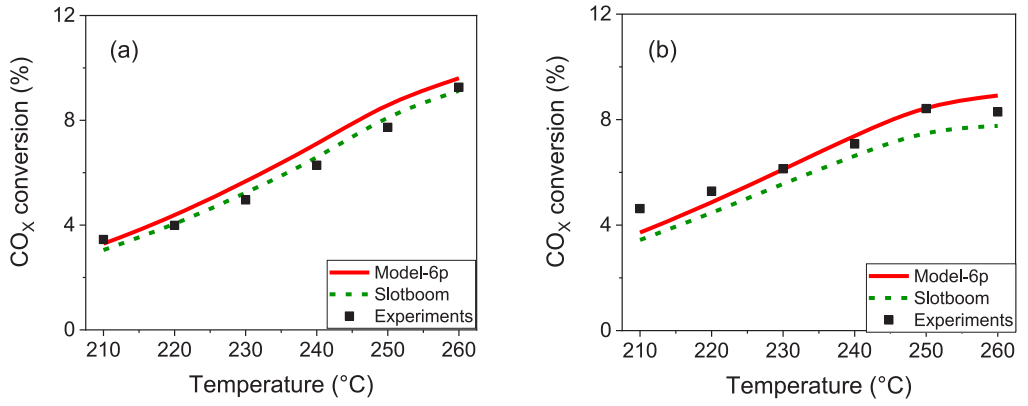

Figure 7. CO_X conversion: simulation vs experiments reported by Campos et al.[14] All experiments are performed at 41 bar. (a) GHSV = 40 $L \cdot h^{-1} \cdot g_{cat}^{-1}$, $H_2/CO/CO_2$ (feed) = 45.3/5.9/8.5% v/v. (b) GHSV = 32 $L \cdot h^{-1} \cdot g_{cat}^{-1}$, $H_2/CO/CO_2$ (feed) = 45.1/4.4/10.4% v/v.

the following elementary equilibrium constants (contained in Model 1p):

$$\overline{K_1} = K_1^{0.5} K_4 K_{12} \tag{25}$$

$$\overline{K_2} = K_1^{0.5} K_5 K_{13} \tag{26}$$

$$\overline{K_3} = K_1^{-0.5} K_8 K_9 \tag{27}$$

Elementary equilibrium constants are usually described by exponential Van't Hoff type expressions ($e^{a+b/T}$), with a and b as constants. After testing this expression for K_{1-3} and finding out that the b parameters were not significant, single constants ($A = e^a$) were used instead. Adsorption constants without temperature dependency have also been applied in recently published models.[6,8]

In Model 9p, nine parameters have to be fitted to the experiments: the pre exponential factors A_{1-3}, the activation energies $E_{A,1-3}$, and the adsorption constants K_{1-3}.

2.3. Model-6p: CO Hydrogenation Not Considered. From simulations of the microkinetic model, it was concluded that the contribution of CO direct hydrogenation to the methanol synthesis is only significant at low CO_2 content in feed, because formate (an intermediate species derived from CO_2) binds strongly on the copper surface, almost completely inhibiting CO hydrogenation.[14,17] Therefore, we developed a simplified model (without considering CO hydrogenation) to simulate the methanol synthesis with feeds containing CO_2, and compared with the model with all three reactions (eqs 1−3).

The alternative Model 6p is a reduced version of Model 9p for CO_2 containing feed ($y_{CO_2,0} \geq 0.005$), considering only CO_2 hydrogenation and the rWGSR (eqs 2 and 3). It has initially seven parameters to be estimated (A_{2-3}, $E_{A,2-3}$, K_{1-3}). In this reparametrization, K_1 tends to infinite, and, consequently, θ_a tends to zero. This is probably because CO hydrogenation is not considered, which happens on site a, contributing to the reduction in the statistical significance of K_1. Therefore, the model can be further reduced to six parameters (K_1 is removed), which are re estimated. The final reaction rates are described as follows.

$$r_{CO_2} = \exp\left(A_2 - \frac{E_{A,2}}{RT}\right)\phi_{Zn}\theta_b\theta f_{H_2}^{1.5} f_{CO} \left(1 - \frac{f_{CH_3OH} f_{H_2O}}{f_{H_2}^3 f_{CO_2} K^0_{P,CO_2hyd}}\right) \tag{28}$$

$$r_{rWGSR} = \exp\left(A_3 - \frac{E_{A,3}}{RT}\right)\theta_b\theta_c\phi_{Zn} f_{CO_2} f_{H_2O} \left(1 - \frac{f_{CO} f_{H_2O}}{f_{H_2} f_{CO_2} K^0_{P,rWGSR}}\right) \tag{29}$$

In Model 6p, six parameters have to be estimated: the pre exponential factors A_{2-3}, the activation energies $E_{A,2-3}$, and the adsorption constants K_{2-3}.

2.4. Reactor Modeling and Parameter Estimation. An experimental database from three different sources was used,[6,8,14] consisting of 557 data points. Of that, 80% of the data from each source was randomly selected as training experiments for parameter estimation, while the remaining 20% were used only for model validation. The operating conditions of the experiments are listed in Table 1, and it was reported that no significant amounts of side products were detected (that is, side reactions are neglected in the kinetic models).

The experiments reported by Campos et al.[14] and Slotboom et al.[8] were performed in a fixed bed tube reactor. Since the reactors used are thin (12 and 6 mm, respectively) and solid inert material was used to dilute the catalyst, isothermal operation is considered (variations smaller than 2 K are reported). As the catalyst particles are significantly small ($c_p \leq 500\ \mu m$), mass transfer limitations are neglected. The influence of back mixing is also neglected (assumption of plug flow reactor, PFR), and only variations along the reactor length are considered.

Derived from mass balances, ordinary differential equations describe the total mole flow ($\dot{n}$) and the mole fractions of each gas component i (y_i) along the reactor length (L):

$$\frac{d\dot{n}}{dz} = \frac{m_{cat}}{L}(-2r_{CO} - 2r_{CO_2}) \tag{30}$$

$$\frac{dy_i}{dz} = \frac{m_{cat}}{L\dot{n}}\sum_{k=1}^{3}(\nu_{i,k} r_k) - y_i\frac{d\dot{n}}{dz} \tag{31}$$

where m_{cat} is the total catalyst mass in the reactor, and $\nu_{i,k}$ is the stoichiometric gain of gas component i in reaction k. The integration of eqs 30 and 31 along the reactor length is made with Matlab function *ode45*, with absolute and relative tolerances of 10^{-8}.

The experiments reported by Seidel et al.[6] were performed in a modified continuous stirred tank reactor (CSTR) (Micro Berty reactor type). Perfect mixture is assumed, and heat and

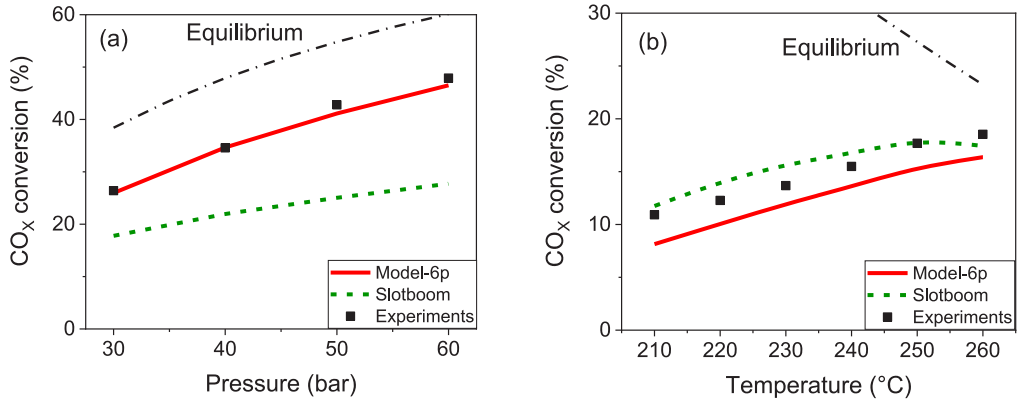

Table 4. Comparison of Statistical Values for the Models Considering Feeds Containing CO_2 ($y_{CO_2,0} \geq 0.001$)

	Model-6p	Slotboom B
no. of fitted parameters	6	6
χ^2 all points (496 pts)	16.9	42.2
χ^2 feed: $H_2/CO/CO_2$ (370 pts)	4.7	29.9
χ^2 feed: H_2/CO_2 (126 pts)	12.3	12.4
$\chi^2_{\text{Orig. Par.}}$ all points (496 pts)		255.3
MSE All Points (496 pts)	0.0114	0.0284
MSE feed: $H_2/CO/CO_2$ (370 pts)	0.0042	0.0269
MSE feed: H_2/CO_2 (126 pts)	0.0325	0.0327
MSE training (80% of the pts)	0.0105	0.0272
MSE validation (20% of the pts)	0.0150	0.0332

mass transfer limitations are neglected. Applying global and component mass balances, the following algebraic equations are obtained:

$$\dot{n}_{out} = \dot{n}_{in} + m_{cat}(-2r_{CO} - 2r_{CO_2}) \tag{32}$$

$$\dot{n}_{in}y_{i,in} - \dot{n}_{out}y_{i,out} + m_{cat}\sum_{k=1}^{3}(\nu_{i,k}r_k) = 0 \tag{33}$$

Here, the subscripts "in" and "out" refer to the flow entering and leaving the reactor, respectively. This nonlinear algebraic system is solved with Matlab function *fsolve*, with a tolerance for both the function and the variables of 10^{-8}.

To estimate the kinetic parameters of each model, an optimization problem is created. Its objective function is the minimization of the normalized squared errors of the prediction of the carbon containing compounds (CO, CO_2, and CH_3OH), the so called chi square (χ^2) regression method (eq 34). The normalization with the inverse of the squared experimental values gives a better weight distribution of the points.[31,32] For points without CO_2 in feed, only the error of CO and CH_3OH are considered.

$$\chi^2 = \sum_{i=1}^{N_p}\left[\frac{(y^i_{CO,out} - \hat{y}^i_{CO,out})^2}{(y^i_{CO,out})^2} + \frac{(y^i_{CH_3OH,out} - \hat{y}^i_{CH_3OH,out})^2}{(y^i_{CH_3OH,out})^2}\right] + \sum_{i=1}^{N_p^*}\left[\frac{(y^i_{CO_2,out} - \hat{y}^i_{CO_2,out})^2}{(y^i_{CO_2,out})^2}\right] \tag{34}$$

Here, N_p is the total number of points, N_p^* is the number of points with CO_2 in feed, $y^i_{j,out}$ is the experimental value of the output mole fraction of gas j in point i, and $\hat{y}^i_{j,out}$ is the simulated value of the output mole fraction of gas j in point i.

The optimization problem is solved with the Matlab function *fmincon* in order to constrain the variables to positive values, with a tolerance for both the function and the variables of 10^{-3}. For Model 1p, the first initial guess of $n_{M,Cat}$ is the value reported in the microkinetic model (2 mol·kg_{cat}^{-1}), while for Model 6p and Model 9p the initial guesses of the parameters are taken by deducing them from Model 1p (eqs 16–21 and eqs 25–27).

In an effort to find the global optimum and not only a local optimum solution, the optimization problem is solved several times, each time changing the initial guesses of multiple variables simultaneously.

The confidence interval of each parameter is obtained with the Matlab function *nlparci*, considering a valid t distribution and 95% confidence. The mean squared error values for all points (MSE) are calculated as follows.

$$\text{MSE} = \frac{1}{2N_p + N_p^*}\left\{\sum_{i=1}^{N_p}\left[\frac{(y^i_{CO,out} - \hat{y}^i_{CO,out})^2}{(y^i_{CO,out})^2} + \frac{(y^i_{CH_3OH,out} - \hat{y}^i_{CH_3OH,out})^2}{(y^i_{CH_3OH,out})^2}\right] + \sum_{i=1}^{N_p^*}\left[\frac{(y^i_{CO_2,out} - \hat{y}^i_{CO_2,out})^2}{(y^i_{CO_2,out})^2}\right]\right\} \tag{35}$$

The new developed kinetic models are compared with the most accurate literature models (according to a recent model comparison[8]), which are the models of Seidel et al.[6] and Slotboom et al.[8] The parameters of these literature models are re estimated according to the procedure described above, in order to ensure a fair comparison. In the model of Seidel et al.,[6] some variables are allowed to have negative values, due to the modified Arrhenius equation and the zinc coverage estimation. Kinetic parameters previously reported by the authors are used as initial guesses, and the procedure of solving the optimization many times by changing the initial guesses is repeated here.

Details of the parameter estimation of all models are summarized in Table 2. The parameters of the model of Slotboom et al.[8] were re estimated two times: once with all points (Slotboom A) (for comparison with Model 1p and 9p) and once with points in which $y_{CO_2,0} \geq 0.001$ (Slotboom B) (for comparison with Model 6p).

Table 5. Equations Summary of the New Developed Model 1p

Model-1p
recommended operating range: $0.05 \leq \bar{y}_{CO_2,0} \leq 0.65$

$$r_{CO} = k_{CO} n_{M,Cat} \theta_a \theta_b f_{H_2} f_{CO} \left(1 - \frac{f_{CH_3OH}}{f_{H_2}^2 f_{CO} K^0_{P,COhyd}}\right) \quad (36)$$

$$r_{CO_2} = k_{CO_2} n_{M,Cat} \theta_b \theta_c f_{H_2}^{1.5} f_{CO} \left(1 - \frac{f_{CH_3OH} f_{H_2O}}{f_{H_2}^3 f_{CO_2} K^0_{P,CO_2hyd}}\right) \quad (37)$$

$$r_{rWGSR} = k_{rWGSR} n_{M,Cat} \theta_c [\theta_a K_A + \theta_b K_B] f_{CO_2} f_{H_2O} \left(1 - \frac{f_{H_2} f_{CO_2}}{f_{CO} f_{H_2O} K^0_{P,WGSR}}\right) \quad (38)$$

$$\theta_a = (K_C f_{CO} + K_D f_{H_2}^{0.5} f_{CO_2} + 1)^{-1} \quad (39)$$

$$\theta_b = (K_E f_{H_2}^{0.5} f_{CO_2} + K_E f_{H_2}^{-0.5} f_{CH_3OH} + 1)^{-1} \quad (40)$$

$$\theta_c = (K_G f_{H_2}^{0.5} + K_H f_{H_2}^{-0.5} f_{H_2O} + 1)^{-1} \quad (41)$$

$$k_{CO} = (1 - \phi_{Zn}) k_{11}^+ K_1 K_2 K_{10} = T^{0.103} \exp(-4632.9T^{-1} - 2.934) \quad (42)$$

$$k_{CO_2} = \phi_{Zn} k_{17}^+ K_1^{1.5} K_5 K_{13} K_{15} = T^{-0.234} \exp(191.2T^{-1} - 7.122) \quad (43)$$

$$k_{rWGSR} = k_{24}^- K_8 = T^{1.875} \exp(-3561.3T^{-1} - 2.776) \quad (44)$$

$$K_A = (1 - \phi_{Zn}) K_4 = T^{-0.258} \exp[-17.233 + 6289.0T^{-1}] \quad (45)$$

$$K_B = \phi_{Zn} K_5 = T^{-0.498} \exp[-15.637 + 6204.9T^{-1}] \quad (46)$$

$$K_C = K_2 = \exp[-19.031 + 7020.3T^{-1}] \quad (47)$$

$$K_D = K_1^{0.5} K_4 K_{12} = T^{-0.756} \exp[-20.480 + 11535.3T^{-1}] \quad (48)$$

$$K_E = K_1^{0.5} K_5 K_{13} = T^{-1.234} \exp[-17.288 + 13049.6T^{-1}] \quad (49)$$

$$K_F = K_1^{-0.5} K_7^{-1} = T^{0.736} \exp[-33.533 + 9702.4T^{-1}] \quad (50)$$

$$K_G = K_1^{0.5} = \exp[-7.274 + 1409.6T^{-1}] \quad (51)$$

$$K_H = K_1^{-0.5} K_8 K_9 = T^{1.036} \exp[-18.450 + 5390.6T^{-1}] \quad (52)$$

$$K^0_{P,COhyd} = T^{-3.384} \exp(10092.4T^{-1} - 4.200) \quad (53)$$

$$K^0_{P,CO_2hyd} = T^{-4.481} \exp(4755.7T^{-1} + 8.369) \quad (54)$$

$$K^0_{P,rWGSR} = T^{-1.097} \exp(-5337.4T^{-1} + 12.569) \quad (55)$$

$$n_{M,Cat} = (1.559 \pm 0.107)\ \text{mol}\cdot\text{kg}_{cat}^{-1} \quad \text{(Fitted parameter)}$$

3. RESULTS AND DISCUSSION

The new developed models and the literature models[6,8] were implemented, and the estimation of the parameters was successful. The discussion is divided between models consid ering the whole operating region (Model 1p Model 9p, Seidel, Slotboom A), and those models considering feeds containing CO_2 (Model 6p, Slotboom B).

3.1. Models Considering the Whole Operating Region.

In Table 3, statistics of the kinetic model regressions considering the whole operating region ($0 \leq y_{CO_2,0} \leq 1$) are summarized. Model 1p has expectedly the highest χ^2 (69.3), as it only has one fitted parameter. However, the greatest part of χ^2 is concentrated on specific operating conditions, such as H_2/CO in feed (χ^2 = 9.6 for 61 points) and particularly H_2/CO_2 in feed (χ^2 = 45.5 for 126 points), while for mixed feed conditions ($H_2/CO/CO_2$ in feed) the experiments are predicted adequately (χ^2 = 14.1 for 370 points). In the latter conditions, the χ^2 of Model 1p is similar to the one of the microkinetic model (13.6), and less than one third of the χ^2 of Slotboom et al.[8] (47.2), which has five more fitted parameters (six in total). The performance of Model 1p at mixed feed conditions is even comparable to the 12 parameter model of Seidel et al.[6] (χ^2 = 9.0).

Model 9p simulates the whole range of conditions with low errors (χ^2 = 22.3), similarly to that of Seidel et al.[6] (24.7), although the latter has three fitted parameters more (12 in total). Looking into the different conditions separately, Model 9p excels at mixed feed conditions (MSE = 0.0066), but also performs well at H_2/CO (MSE = 0.0280) and H_2/CO_2 feed conditions (MSE = 0.0304).

For all considered models, the MSE of the training set is relatively close to its respective MSE of the validation set, suggesting that interpolations inside the validated operating region are consistent.

In Figure 1 and Figure 2, parity plots of Model 1p and Model 9p are shown, respectively. From Figure 1d and 1e, it can be seen that Model 1p shows discrepancies in the simulation of methanol output concentration at conditions with H_2/CO or H_2/CO_2 in feed. However, Model 1p accurately simulates mixed feed experiments, with most of these points being inside

the ±20% lines (99% of CO, 100% of CO_2, and 73% of CH_3OH points).

In Figure 2, it is shown that Model 9p simulations are in good agreement with the experiments in the whole range of conditions, with 93% of CO, 100% of CO_2, and 79% of CH_3OH points being inside the ±20% lines. Parity plots of the literature models considered in this work are available in the Supporting Information (Figures S1 and S3).

Experimental and simulated data of methanol output concentration at different operating conditions are shown in Figures 3–5. Model 1p accurately predicts trends at low CO_2/CO_x feed concentration ($y_{CO_2,0}$), either at low CO_x conversion (Figure 3a,b) or at high CO_x conversion (Figure 4a,b). By higher $y_{CO_2,0}$, underestimations at low temperature and overestimations at high temperature are recognized, with small deviations at $y_{CO_2,0} = 0.50$ (Figure 3c), and higher deviations at $y_{CO_2,0} \geq 0.70$ (Figures 3d and 5a). Still, the model correctly describes conditions of $y_{CO_2,0} = 1$ at low temperature (220 °C, Figure 5b). In general, the trends simulated by Model 1p look similar to those of the underlying microkinetic model. This confirms that the model reduction was successful, and most of the theoretical information was kept in the new model.

The reparametrized model of Slotboom et al.[8] (Slotboom A) shows reasonable agreement to experimental data at low CO_x conversion (Figures 3a,d and 5ab), with some underestimations, as in Figure 3a,d, and some overestimations, as in Figure 5b. At high CO_x conversion, however, there are high systematic deviations (see Figure 4a,b).

Both Model 9p and model of Seidel et al.[6] show excellent agreement at low CO_x conversion (Figure 3a–d), and reasonable agreement at $y_{CO_2,0} = 1$ (Figure 5a,b). At high CO_x conversion (Figure 4a,b), some underestimations are seen in both cases, with the simulations of the Model 9p being closer to the experimental data.

3.2. Models Considering Operation with CO_2 in Feed.

In Table 4, statistics for Model 6p and the Slotboom B model are summarized. Model 6p had a $\chi^2 = 16.9$ for the 496 data points, which is less than half the value of Slotboom B ($\chi^2 = 42.2$). While their performance is similar at H_2/CO_2 feed conditions ($\chi^2 = 12.3$ and $\chi^2 = 12.4$, respectively), significantly different simulation results are seen in the mixed feed conditions, with Model 6p showing a superior performance ($\chi^2 = 4.7$) in comparison with Slotboom B ($\chi^2 = 29.9$).

Model 6p has a similar performance to Model 9p and to Seidel's model for experiments with H_2/CO_2 in feed ($\chi^2_{6p} = 12.3$, $\chi^2_{9p} = 11.5$, and $\chi^2_{Seidel} = 11.6$), and a significantly better performance at simulating mixed feed conditions ($\chi^2_{6p} = 4.7$, $\chi^2_{9p} = 7.4$, and $\chi^2_{Seidel} = 9.0$). It is important to mention that Model 9p and Seidel's model are also simulating experiments with H_2/CO in feed, and, therefore, the comparison with Model 6p is not completely fair. Still, there is a remarkable performance for a model which has only six parameters, comparing with the nine parameters of Model 9p and the 12 parameters of Seidel's model.

In Figure 6, parity plots of the Model 6p are shown. Deviations follow a narrow distribution, with the majority of the simulations having an error lower than ±20% (94% of CO, 100% of CO_2, and 86% of CH_3OH points). Parity plots of the Slotboom B model are provided in the Supporting Information (Figure S2).

Table 6. Equations Summary of the New Developed Model 6p

Model-6p
recommended operating range: $\bar{y}_{CO_2,0} \geq 0.35$

$$r_{CO_2} = \exp\left(A_2 - \frac{E_{A,2}}{RT}\right)\phi_{Zn}\theta_b\theta_c f_{H_2}^{1.5} f_{CO}\left(1 - \frac{f_{CH_3OH} f_{H_2O}}{f_{H_2}^3 f_{CO_2} K^0_{P,CO_2hyd}}\right) \quad (56)$$

$$r_{rWGSR} = \exp\left(A_3 - \frac{E_{A,3}}{RT}\right)\theta_b\theta_c\phi_{Zn} f_{CO_2} f_{H_2O}\left(1 - \frac{f_{CO} f_{H_2O}}{f_{H_2} f_{CO_2} K^0_{P,rWGSR}}\right) \quad (57)$$

$$\theta_b = (\overline{K_2} f_{H_2}^{0.5} f_{CO_2} + 1)^{-1} \quad (58)$$

$$\theta_c = (\overline{K_3} f_{H_2}^{-0.5} f_{H_2O} + 1)^{-1} \quad (59)$$

$$\text{if } \bar{y}_{CO_2,0} \leq 0.90 \quad \phi_{Zn} = 0.50$$

$$\text{if } \bar{y}_{CO_2,0} > 0.90 \quad \phi_{Zn} = 0.10 \quad (60)$$

Fitted Parameters

$A_2 = 14.41 \pm 0.99$ $A_3 = 29.13 \pm 1.74$

$E_{A,2} = (94.73 \pm 4.18)$ kJ·mol^{-1} $E_{A,3} = (132.79 \pm 7.46)$ kJ·mol^{-1}

$\overline{K_2} = (0.1441 \pm 0.0289)$ bar$^{-1.5}$ $\overline{K_3} = (49.44 \pm 11.08)$ bar$^{-0.5}$

Table 7. Equations Summary of the New Developed Model 9p

Model-9p
recommended operating range: $0 \leq \bar{y}_{CO_2,0} \leq 1$

$$r_{CO} = \exp\left(A_1 - \frac{E_{A,1}}{RT}\right)(1 - \phi_{Zn})\theta_a\theta_c f_{H_2} f_{CO}\left(1 - \frac{f_{CH_3OH}}{f_{H_2}^2 f_{CO} K^0_{P,COhyd}}\right) \quad (61)$$

$$r_{CO_2} = \exp\left(A_2 - \frac{E_{A,2}}{RT}\right)\phi_{Zn}\theta_b\theta_c f_{H_2}^{1.5} f_{CO}\left(1 - \frac{f_{CH_3OH} f_{H_2O}}{f_{H_2}^3 f_{CO_2} K^0_{P,CO_2hyd}}\right) \quad (62)$$

$$r_{rWGSR} = \exp\left(A_3 - \frac{E_{A,3}}{RT}\right)\theta_c[(1 - \phi_{Zn})\theta_a + \phi_{Zn}\theta_b] f_{CO_2} f_{H_2O}\left(1 - \frac{f_{CO} f_{H_2O}}{f_{H_2} f_{CO_2} K^0_{P,rWGSR}}\right) \quad (63)$$

$$\theta_a = (\overline{K_1} f_{H_2}^{0.5} f_{CO_2} + 1)^{-1} \quad (64)$$

$$\theta_b = (\overline{K_2} f_{H_2}^{0.5} f_{CO_2} + 1)^{-1} \quad (65)$$

$$\theta_c = (\overline{K_3} f_{H_2}^{-0.5} f_{H_2O} + 1)^{-1} \quad (66)$$

$$\text{if } \bar{y}_{CO_2,0} \leq 0.001 \quad \phi_{Zn} = 0.95$$

$$\text{if } 0.001 \leq \bar{y}_{CO_2,0} \leq 0.90 \quad \phi_{Zn} = 0.50$$

$$\text{if } \bar{y}_{CO_2,0} > 0.90 \quad \phi_{Zn} = 0.10 \quad (67)$$

Fitted Parameters

$A_1 = 11.459 \pm 3.661$ $A_2 = 20.974 \pm 2.012$ $A_3 = 32.083 \pm 2.163$

$E_{A,1} = (90.65 \pm 16.57)$ kJ·mol^{-1} $E_{A,2} = (112.09 \pm 5.81)$ kJ·mol^{-1}

$E_{A,3} = (137.33 \pm 7.46)$ kJ·mol^{-1} $\overline{K_1} = (0.968 \pm 0.393)$ bar$^{-1.5}$

$\overline{K_2} = (0.0489 \pm 0.0091)$ bar$^{-1.5}$ $\overline{K_3} = (1420 \pm 2049)$ bar$^{-0.5}$

Experimental and simulated values of methanol output concentration for different operating conditions are shown in Figure 7 and Figure 8. Model 6p adequately predicts the trends

for all operating conditions, while the Slotboom B model has significant deviations at high CO_x conversion (Figure Sa).

3.3. Summary of the Models. All necessary equations and optimized parameters for the implementation of the three developed models (Model 1p, Model 6p, Model 9p) are summarized in Tables 5-7.

4. CONCLUSIONS

Three kinetic models (Model 1p, Model 6p, and Model 9p) were developed, validated, and compared with other models from the literature.

If the operating region of interest involves feeds with and without CO_2 ($0 < y_{CO,o} < 1$), then Model 9p is the most suitable, since it exhibited a small χ^2, a moderate amount of estimated parameters (9), and exhibits adequate trends for different conditions.

If the operating region contains low to moderate CO_2 content in feed ($0.05 < y_{CO,o} < 0.65$), then Model 1p is recommended, since its χ^2 is low, trends are adequately represented, and there is only one fitted parameter. In the whole range of studied conditions, the simulations performed with Model 1p are similar to those using the more complex microkinetic model, hence, confirming that the model reduction was successful, and most of the theoretical information was kept in the reduced model

Finally, if the operating range considers CO_2 containing feeds ($y_{CO,o} \geq 0.001$), then Model 6p offers the best fit. This model has the lowest χ^2 of the analyzed models, has a low amount of fitted parameters (6) and two global reactions.

The new models should efficiently simulate the methanol synthesis at various operating conditions, while also being suitable for reactor optimization and process scale up.

An additional contribution of this work is the re estimation of the parameters of literature models using a larger experimental database, increasing the validated operating window of these kinetic models. These re estimated parameters are provided in the Supporting Information.

ASSOCIATED CONTENT

Supporting Information

The Supporting Information is available free of charge at https://pubs.acs.org/doi/10.1021/acs.iecr.lc02952.

Mathematical derivation of the kinetic equations; kinetic constants, equilibrium constants, and zinc coverage; parameter re estimation of the model from Slotboom et al;[8] original and optimized kinetic parameters from Slotboom et al.[8]; additional figures that support the text (PDF)

AUTHOR INFORMATION

Corresponding Author

Karla Herrera Delgado - *Institute for Catalysis Research and Technology (IKFT), Karlsruhe Institute of Technologie (KIT), 76344 Eggenstein Leopoldshafen, Gennany;* orcid.org/0000 0003 1889 3719; Phone: +49 721 608 28631; Email: karla.herrera@)kit.edu

Authors

Bruno Lacerda de Oliveira Campos - *Institute for Catalysis Research and Technology (IKFT), Karlsruhe Institute of Technologie (KIT), 76344 Eggenstein Leopoldshafen, Gennany*

Stephan Pitter - *Institute for Catalysis Research and Technology (IKFT), Karlsruhe Institute of Technologie (KIT), 76344 Eggenstein Leopoldshafen, Germany*

Jörg Sauer - *Institute for Catalysis Research and Technology (IKFT), Karlsruhe Institute of Technologie (KIT), 76344 Eggenstein Leopoldshafen, Gennany;* orcid.org/0000 0003 3133 4110

Notes

The authors declare no competing financial interest.

ACKNOWLEDGMENTS

The authors thank Coordena o de Aperfei oamento de Pessoal de Nivel Superior (CAPES) for financing the Ph.D. scholarship ofB.L.O.C. (Process No. 88881.174609/2018 01). The authors acknowledge the financial support from the Helmholtz Research Program "Materials and Technologies for the Energy Transition (MTET), Topic 3: Chemical Energy Carriers".

NOMENCLATURE

A_n = Parameter n of Model 9p and Model 6p

$A_{n,m}$ = Coefficient n of the equilibrium constant of global reaction m

$E_{A,m}$ = Activation energy of global reaction m {kJ·moJ-1) $E_{A,k}$ = Forward activation energy of elementary reaction k (kJ· moJ-1)

$E_{A,-k}$ = Reverse activation energy of elementary reaction k (k) • mol-1)

f_j = Fugacity of gas component j (Pa)

h = Planck constant (6.62607 X 10-34 J-s)

K_k = Equilibrium constant of elementary step k (-)

K = Parameter with lumped equilibrium constants ( )

K_m = Equilibrium constant of global reaction m (-)

k_B =Boltzmann constant (1.38065 X 10^{-23} J-K-1)

k_k = Rate constant ofreaction k (s-1)

L = Reactor length (m)

m_{cat} = Total catalyst mass (kg)

MSE = Mean squared error (-)

n =Totalmole flow (mol·s 1)

N_g = Number of gas components (-)

NP = Number of experimental points (-)

N_i = Number of experimental points with CO_2 in feed (-)

$n_{M,Cat}$ = Specific catalyst site quantity (mol·kg-1)

R = Universalgas constant (0.0083144598 kJ·moJ-1-K-1)

r_{k*} = Reaction rate of reversible reaction k (s-1)

βS_k = Entropy barrier of elementary reaction k {kJ·moJ-1· K-1)

T = Temperature (K)

y_j = Mole fraction of gas component j

$y_{j,out}$ = Experimental output mole fraction of gas component j at operating point i

$Y_{j,out}$ = Simulated output mole fraction of gas component j at operating point i

Greek

β_k = Correction term of reaction k because of the thermodynamic consistency (-)

θ_i = Surface coverage of species i (-)

ν'_{ik} = Stoichiometric coefficient of reactant i in reaction k (-)

ν''_{ik} = Stoichiometric coefficient of product i in reaction k (-)

ν_{ik} = Stoichiometric gain of gas component i in reaction k (-)

ϕ_{Zn} = Zinc coverage on the catalyst surface
χ^2 = Sum of squared errors (chi square regression method)

Subscripts

in = Entering the reactor
out = Leaving the reactor

Superscripts

+ = Forward reaction
− = Reverse reaction

REFERENCES

(1) Dalena, F.; Senatore, A.; Marino, A.; Gordano, A.; Basile, M.; Basile, A., Chapter 1 Methanol Production and Applications: An Overview. In *Methanol*; Basile, A., Dalena, F., Eds.; Elsevier: 2018; pp 3−28.

(2) Dahmen, N.; Henrich, E.; Dinjus, E.; Weirich, F. The bioliq® bioslurry gasification process for the production of biosynfuels, organic chemicals, and energy. *Energy, Sustainability and Society* **2012**, *2* (1), 3.

(3) Hansen, J. B.; Nielsen, P. E. H., Methanol Synthesis. In *Handbook of Heterogeneous Catalysis*, 2nd ed.; Knözinger, G. E. H., Schüth, F., Weitkamp, J., Ed.; Wiley: **2008**; pp 2920−2949.

(4) Graaf, G. H.; Stamhuis, E. J.; Beenackers, A. A. C. M. Kinetics of low pressure methanol synthesis. *Chem. Eng. Sci.* **1988**, *43* (12), 3185−3195.

(5) Bussche, K. M. V.; Froment, G. F. A Steady State Kinetic Model for Methanol Synthesis and the Water Gas Shift Reaction on a Commercial Cu/ZnO/Al2O3Catalyst. *J. Catal.* **1996**, *161* (1), 1−10.

(6) Seidel, C.; Jörke, A.; Vollbrecht, B.; Seidel Morgenstern, A.; Kienle, A. Kinetic modeling of methanol synthesis from renewable resources. *Chem. Eng. Sci.* **2018**, *175*, 130−138.

(7) Ovesen, C. V.; Clausen, B. S.; Schiøtz, J.; Stoltze, P.; Topsøe, H.; Nørskov, J. K. Kinetic Implications of Dynamical Changes in Catalyst Morphology during Methanol Synthesis over Cu/ZnO Catalysts. *J. Catal.* **1997**, *168* (2), 133−142.

(8) Slotboom, Y.; Bos, M. J.; Pieper, J.; Vrieswijk, V.; Likozar, B.; Kersten, S. R. A.; Brilman, D. W. F. Critical assessment of steady state kinetic models for the synthesis of methanol over an industrial Cu/ZnO/Al2O3 catalyst. *Chem. Eng. J.* **2020**, *389*, 124181.

(9) Grabow, L. C.; Mavrikakis, M. Mechanism of Methanol Synthesis on Cu through CO2 and CO Hydrogenation. *ACS Catal.* **2011**, *1* (4), 365−384.

(10) Park, J.; Cho, J.; Lee, Y.; Park, M. J.; Lee, W. B. Practical Microkinetic Modeling Approach for Methanol Synthesis from Syngas over a Cu Based Catalyst. *Ind. Eng. Chem. Res.* **2019**, *58* (20), 8663−8673.

(11) Xu, D.; Wu, P.; Yang, B. Essential Role of Water in the Autocatalysis Behavior of Methanol Synthesis from CO2 Hydro genation on Cu: A Combined DFT and Microkinetic Modeling Study. *J. Phys. Chem. C* **2019**, *123* (14), 8959−8966.

(12) Janse van Rensburg, W.; Petersen, M. A.; Datt, M. S.; van den Berg, J. A.; van Helden, P. On the Kinetic Interpretation of DFT Derived Energy Profiles: Cu Catalyzed Methanol Synthesis. *Catal. Lett.* **2015**, *145* (2), 559−568.

(13) Huš, M.; Kopač, D.; Štefančič, N. S.; Jurković, D. L.; Dasireddy, V. D. B. C.; Likozar, B. Unravelling the mechanisms of CO2 hydrogenation to methanol on Cu based catalysts using first principles multiscale modelling and experiments. *Catal. Sci. Technol.* **2017**, *7* (24), 5900−5913.

(14) Lacerda de Oliveira Campos, B.; Herrera Delgado, K.; Wild, S.; Studt, F.; Pitter, S.; Sauer, J. Surface reaction kinetics of the methanol synthesis and the water gas shift reaction on Cu/ZnO/Al2O3. *Reaction Chemistry & Engineering* **2021**, *6* (5), 868−887.

(15) Behrens, M.; Studt, F.; Kasatkin, I.; Kühl, S.; Hävecker, M.; Abild Pedersen, F.; Zander, S.; Girgsdies, F.; Kurr, P.; Kniep, B. L.; Tovar, M.; Fischer, R. W.; Nørskov, J. K.; Schlögl, R. The Active Site of Methanol Synthesis over Cu/ZnO/Al22O33 Industrial Catalysts. *Science* **2012**, *336* (6083), 893−897.

(16) Studt, F.; Behrens, M.; Abild Pedersen, F. Energetics of the Water−Gas Shift Reaction on the Active Sites of the Industrially Used Cu/ZnO/Al2O3 Catalyst. *Catal. Lett.* **2014**, *144* (11), 1973−1977.

(17) Studt, F.; Behrens, M.; Kunkes, E. L.; Thomas, N.; Zander, S.; Tarasov, A.; Schumann, J.; Frei, E.; Varley, J. B.; Abild Pedersen, F.; Nørskov, J. K.; Schlögl, R. The Mechanism of CO and CO2 Hydrogenation to Methanol over Cu Based Catalysts. *ChemCatChem* **2015**, *7* (7), 1105−1111.

(18) de Oliveira, L. P.; Hudebine, D.; Guillaume, D.; Verstraete, J. J. A Review of Kinetic Modeling Methodologies for Complex Processes. *Oil Gas Sci. Technol.* **2016**, *71* (3), 45.

(19) Park, J.; Kim, H. S.; Lee, W. B.; Park, M. J. Trends and Outlook of Computational Chemistry and Microkinetic Modeling for Catalytic Synthesis of Methanol and DME. *Catalysts* **2020**, *10* (6), 655.

(20) Campbell, C. T. The Degree of Rate Control: A Powerful Tool for Catalysis Research. *ACS Catal.* **2017**, *7* (4), 2770−2779.

(21) Peng, D. Y.; Robinson, D. B. A New Two Constant Equation of State. *Ind. Eng. Chem. Fundam.* **1976**, *15* (1), 59−64.

(22) Meng, L.; Duan, Y. Y. Prediction of the second cross virial coefficients of nonpolar binary mixtures. *Fluid Phase Equilib.* **2005**, *238* (2), 229−238.

(23) Meng, L.; Duan, Y. Y.; Wang, X. D. Binary interaction parameter kij for calculating the second cross virial coefficients of mixtures. *Fluid Phase Equilib.* **2007**, *260* (2), 354−358.

(24) Deiters, U. K. Comments on the modeling of hydrogen and hydrogen containing mixtures with cubic equations of state. *Fluid Phase Equilib.* **2013**, *352*, 93−96.

(25) Herrera Delgado, K.; Maier, L.; Tischer, S.; Zellner, A.; Stotz, H.; Deutschmann, O. Surface Reaction Kinetics of Steam and CO2 Reforming as Well as Oxidation of Methane over Nickel Based Catalysts. *Catalysts* **2015**, *5*, 871−904.

(26) Stotz, H.; Maier, L.; Boubnov, A.; Gremminger, A. T.; Grunwaldt, J. D.; Deutschmann, O. Surface reaction kinetics of methane oxidation over PdO. *J. Catal.* **2019**, *370*, 152−175.

(27) Goos, E. B. A.; Ruscic, B. New NASA thermodynamic polynomials database. http://garfield.chem.elte.hu/Burcat/THERM.DAT (accessed 2020 08).

(28) Grunwaldt, J. D.; Molenbroek, A. M.; Topsøe, N. Y.; Topsøe, H.; Clausen, B. S. In Situ Investigations of Structural Changes in Cu/ZnO Catalysts. *J. Catal.* **2000**, *194* (2), 452−460.

(29) Kuld, S.; Thorhauge, M.; Falsig, H.; Elkjær, C. F.; Helveg, S.; Chorkendorff, I.; Sehested, J. Quantifying the promotion of Cu catalysts by ZnO for methanol synthesis. *Science* **2016**, *352* (6288), 969−974.

(30) Lacerda de Oliveira Campos, B.; Herrera Delgado, K.; Wild, S.; Studt, F.; Pitter, S.; Sauer, J. Correction: Surface reaction kinetics of the methanol synthesis and the water gas shift reaction on Cu/ZnO/Al2O3. *Reaction Chemistry & Engineering* **2021**, *6* (8), 1483−1486.

(31) Lacerda de Oliveira Campos, B.; Oliveira Souza da Costa, A.; Ferreira da Costa Junior, E. Mathematical modeling and sensibility analysis of a solar humidification dehumidification desalination system considering saturated air. *Sol. Energy* **2017**, *157*, 321−327.

(32) Lacerda de Oliveira Campos, B.; Oliveira Souza da Costa, A.; Cecília de Souza Figueiredo, K.; Ferreira da Costa Junior, E. Performance comparison of different mathematical models in the simulation of a solar desalination by humidification dehumidification. *Desalination* **2018**, *437*, 184−194.